Numerical investigation of two-phase flow in high-permeability porous media: Effect of permeability variation on the surface force between phases

Maxime Cochennec[1,2], Hossein Davarzani[1], Yohan Davit[2], Ioannis Igniatiadis[1], Michel Quintard[2]

Abstract

The macroscopic description of two-phase flow in porous media requires modeling the force of interaction between the phases, i.e. the two fluids and the solid phase. The flow regimes specific to high permeability porous media are characterized by a non-negligible extent of the interface between the two fluids, compared to the fluid-solid interface. This argues for the systematic introduction of the fluid-fluid interaction terms, i.e. surface integrals also called traction, in the macroscopic momentum equations. However, we do not know whether these terms are always non-negligible for this type of flow regime, for example in cases where the friction with the solid becomes very large. Here we assess that the share of the traction between the fluids in the overall pressure drop increases when the flow is more confined, and thus the friction with the solid phase increases. The idea of solving modified 2D-Stokes equations with a supplementary Darcy term allowed us to modify the absolute permeability of the structure without having to modify the geometry per se. Our results demonstrate that the absolute permeability of

[1]French Geological Survey
[2]Institut de Mécanique des Fluides de Toulouse

the structure does not prejudge the importance of the traction between fluids in the total pressure drop as long as the flow regime is characteristic of flow in high permeability porous media.

---

1. Introduction

1.1. Two-phase flow in high-permeability porous media

An accurate description of two-phase flow in high-permeability porous media is of major importance for several practical applications. One can mention, among others, soil remediation in gravely soils (Fetter et al., 2017), nuclear safety (Clavier et al., 2017) or hydrodynamic of catalytic fixed bed reactors (de Santos et al., 1991). However, most of the literature is dedicated to two-phase flow in low-permeability porous media.

Due to the larger pore size, two-phase flow in high-permeability porous media (hereafter, high-permeability porous media refers to media for which the characteristic particle diameter is about one millimeter and above) results in a complex interaction between capillary, gravity and viscous forces (Davit and Quintard, 2018). For low-permeability porous media, the flow is usually dominated by surface tension force, i.e. the capillary number is low, usually inferior to 10^{-3}, and the fluid repartition pattern is well described as two independent flow streams separate by a multitude of stable meniscus at steady state, as illustrated in Fig. 1 (a) (Dullien, 2012). This regime is characterized by the small extent of the fluid-fluid interface, as the fluid phases are segregated, with the wetting phase flowing into the larger pores while the wetting phase occupies the smaller pores. In contrast, for high permeability porous media, the flow is no longer capillary-dominated and the viscous forces become significant (also gravity and inertial effects

may become important if Bond and Reynolds numbers are high, respectively). Thus the fluids repartition patterns can take two forms, either the non-wetting phase is continuous, see as an example Fig. 1 (b), or is flowing as droplets or ganglia, as in Fig. 1 (c). For these two options, the wetting phase is flowing as a film in contact with the solid and the non-wetting phase flows at the center of the pores surrounded by the wetting phase. Strictly speaking, these different regimes must be considered when attempting to describe two-phase flows with continuous macroscopic equations. Indeed, it has been shown several times that the overall flow properties depend on the flow regimes (Avraam and Payatakes, 1995a; Armstrong et al., 2016). At first glance, one would consider that the exchange terms between the fluids, through their common surfaces, as negligible compared to their counterpart between the fluid phases and the solid phase for surface-tension dominated flow since the extent of the fluid-fluid interface is small. On the other hand, and this is what we are interested in here, this is not necessarily the case for regimes specific to flow in high-permeability porous media for which the extent of the fluid-fluid interface is large. This is important because, as discussed in the next section, these exchange terms between phases are the basis of any attempt to establish continuous relationships on a macroscopic scale starting from the pore scale.

1.2. Continuous model

Volume averaged microscopic equation of motion for two Newtonian fluids $i, j = o, w$ reads

$$\rho_i \varepsilon_i \left(\frac{\partial \mathbf{U}_i}{\partial t} + \mathbf{U}_i \cdot \nabla \mathbf{U}_i \right) = -\varepsilon_i \nabla P_i + \varepsilon_i \rho_i \mathbf{g} + \varepsilon_i \nabla \cdot \tau_i + (\mathbf{F}_{ij} + \mathbf{F}_{is}), \; i \neq j, \quad (1)$$

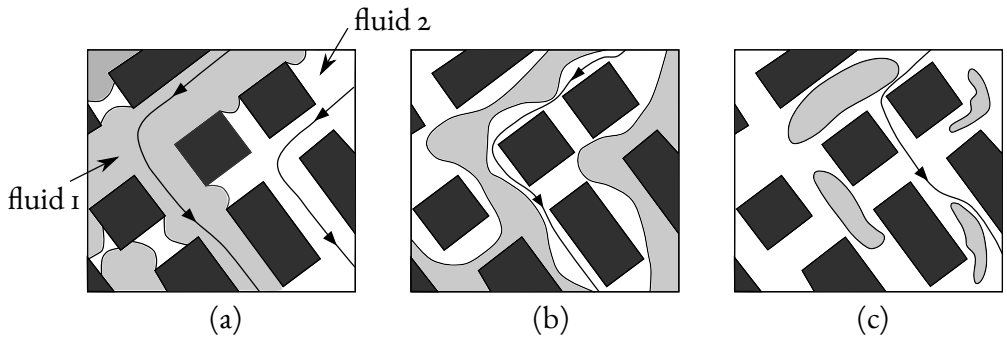

Figure 1: Illustration of possible fluids dispatching in a 2D porous network with solid phase in black, fluid 1, that stands for the non-wetting phase (gray) and the wetting fluid (white), (a) the two fluids are flowing in different channels separate by numerous meniscus (b) wetting and non-wetting fluid are flowing together in most of the pores as two continuous streams and (c) both fluids are flowing together in most of the pores and the non-wetting phase is discontinuous - Adapted from (Dullien, 2012)

where $\varepsilon_i = V_i/V$ is the volume fraction of the i-fluid and V is a representative elementary volume, U_i is the intrinsic average velocity of the i-fluid, P_i is the intrinsic average pressure of the i-fluid and τ_i denotes the average viscous stress tensor. The last two terms in the left hand side denote the force of interaction per unite volume exerted by fluid i upon fluid j and the force of interaction per unit volume exerted by fluid i upon the solid phase, respectively (Kalaydjian, 1987).

From there, there are two possible ways to adress Eq. 1 and the associated equations. In volume averaging litterature, one seeks to express the terms of interaction between the phases with averaged quantities and to recast equation Eq. 1 in a form similar to Darcy's law (equation for creeping saturated single-phase flow in porous media). Indeed, by considering creeping two-phase flow Eq. 1 can be written as

$$0 = -\varepsilon_i \nabla P_i + \varepsilon_i \rho_i \mathbf{g} + \frac{1}{V} \int_{A_{is}+A_{ij}} \mathbf{n}_i \cdot \left(-\mathbf{I} p_i + \mu_i \left(\nabla \mathbf{u}_i + (\nabla \mathbf{u}_i)^T \right) \right) \mathrm{d}A. \quad (2)$$

where p_i and u_i are microscopic pressure and velocity fields of fluid i, respectively. By expressing the surface integrals in term of averaged quantities one can obtain the following momentum balance equations,

$$\mathbf{U}_i = -\frac{1}{\mu_i}\mathbf{K}^*_{ii}\cdot(\nabla P_i - \rho_i\mathbf{g}) - \frac{1}{\mu_j}\mathbf{K}^*_{ij}\cdot(\nabla P_j - \rho_j\mathbf{g}), \quad i,j = o,w \,\text{and}\, i \neq j, \tag{3}$$

in which $\mathbf{K}^*_{ij}$ are the coupled relative permeability tensors that pertain to the interaction between the fluids (Whitaker, 1986; Lasseux et al., 1996).

The reader is warned that Eq. 3 has, to our knowledge, never been used in practice to model two-phase subsurface flows. On the contrary, the ubiquitous continuous model used to describe two-phase flows in soils is based on a direct extension of the Darcy's equation and the whole model, also known as Muskat equations (Wyckoff and Botset, 1936; Muskat, 1938), reads

$$0 = \frac{\partial \varepsilon S_i}{\partial t} + \nabla\cdot\mathbf{U}_i, \quad i = o,w, \tag{4a}$$

$$\mathbf{U}_i = -\frac{1}{\mu_i}\mathbf{K}_i\cdot(\nabla P_i - \rho_i\mathbf{g}), \quad i = o,w, \tag{4b}$$

$$1 = S_w + S_o \tag{4c}$$

$$\mathbf{K}_w = \mathbf{K}k_{rw}(S_w), \qquad \mathbf{K}_o = \mathbf{K}k_{ro}(S_w), \tag{4d}$$

$$P_c(S_w) = P_o - P_w. \tag{4e}$$

where $\mathbf{K}$ is the absolute permeability tensor. The generalization toward two-phase flows involves the introduction of the relative permeability terms k_{ri} which account for the division of the void space between the fluids (Dullien, 2012), thus the relative permeability depends (non-linearly) only on the saturation. To close the set of the macroscopic equations a constitutive relation between the macroscopic pressure of each fluid has to be furnished. This relation is known as the capillary pressure relation and, as for the relative permeabilities, is supposed to depends non-linearly only on the saturation (Leverett et al., 1941).

A significant amount of work attempted to make improvements to the Muskat equations (e.g. including moving contact line (Kalaydjian, 1987; Hassanizadeh and Gray, 1993; Barenblatt et al., 2003) or take into account the trapped phases (Hilfer, 1998)). Here we would stress that the concept of relative permeabilities into the Muskat equations is dedicated to independent flow pathways only (Blunt, 2017) and the underlying assumption that the two streams do not interfere with each other, a situation far from the regimes previously identified for high permeability porous media. Thus Eq. 4(b) does not take into account the interaction between the fluids as opposed to Eq. 3. If the former is used to the detriment of the latter, it is mainly because the literature on subsurface flow is focused on oil recovery applications, for which the permeability is very low and the independent streams regime is a good approximation.

Another approach, widely used in the literature on two-phase flow in Trickle Bed

Reactor (TBR), is to implement Eq. 1 and provide constitutive relations for the interaction terms between the phases. These relations are usually obtained through interpretation of experimental data. Some results, focusing on relation for the interaction between the fluid phases, are given in the next section as well as results in literature for coupled permeabilities from the porous medium approach.

1.3. Modeling of the interaction between fluids

Based on the generalized Darcy law with coupled terms Eq. 3, experimental works computed the coupled transport coefficient through steady-state cocurent flow in sandpack with one fluid, and alternatively the other, which is submitted to a null pressure gradient. This protocol was used with oil and water in a cylindric sandpack (Zarcone and Lenormand, 1994) and the authors found a negligible effect of the coupled permeabilities in the overall flow. With the same protocol, with oil and water in a 2D-sandpack Dullien and Dong (1996) found that the coupled permeabilities are important since they can contribute at best to 35% of the effective permeability. Alternatively, authors imposed (Ramakrishnan and Goode, 2015) a null displacement and measured the induced pressure drop, with air and water in a Berea sandstone core they found that the coupled transport coefficients must not be overlooked for intermediate saturations. Several authors conducted experiments with two different set-ups as proposed by Rose (1988), see for example Bentsen and Manai (1993) who made cocurrent and countercurrent experiments with water and oil in a sandpack and found that coupled permeabilities reach, at least, 15% of the effective permeability value. However, it was pointed out that the saturation between the two sets of experiments can be very dif-

ferent and therefore the computed relative permeabilities can not be safely compared (Langaas and Papatzacos, 2001). The effect of the non-wetting phase connectivity on the transport parameters was extensively studied in (Avraam and Payatakes, 1995b), the authors performed steady-state cocurrent two-phase flow in 2D-micro model experiments and found that the contribution of the coupled permeabilities on the flow is non-negligible and depend on the flow regimes.

Several numerical studies investigated the share of the coupled permeabilities in the effective permeability. The seminal work of Rothman (1990) examined the question by conducting two-phase flow simulations in simple geometries with the immiscible lattice-gas method. The author found non-negligible participation of the coupled permeabilities by applying the volume force alternatively on each fluid. Numerous authors used the lattice-Boltzmann method, such as (Li et al., 2005), in which the authors examined the value of the coupled permeabilities as a function of the saturation in a 3D-sphere pack and they found results in agreement with Rothman's results. Yiotis et al. (2007) used a lattice Boltzmann method in 2D and 3D pore networks and found a non-wetting apparent relative permeability greater than unity when the wetting fluid is more viscous than the non-wetting fluid. This result is a manifestation of the lubrification effect, also observed in experiments (Odeh et al., 1959), and arising because of strong hydraulic coupling between the fluids. Recently, Shams et al. (2018) have used a Volume Of Fluid method to study the transport coefficients of fluid layers in non-circular capillary tubes. Based on analogy with a model Couette flow the authors have derived simple relations that can predict with good accuracy the transport coefficients, including the coupled ones, of fluid layers. We can also refer to recent work in which

a whole analytical model is given for one-dimensional two-phase flow in coarse non-consolidated porous media and which correctly predicts the pressure loss in a debris bed (Clavier et al., 2017).

Several correlations from theorical analysis for the fluid-fluid force interaction have been derived in hydrodynamic of TBR litterature. These correlations usually relate the momentum exchange between the fluids to the flow velocity and the medium properties with Ergun's like relations. For example, Attou et al. (1999) found that the drag between the fluids can be expressed as follows

$$F_{lg} = A_{lg} U_r + B_{lg} U_r^2,$$

where the relative velocity is given by $U_r = U_g - \frac{S_g}{S_l} U_l$ and A_{lg} and B_{lg} are coefficients that depend on the volume fraction of the gas phase and the medium properties. The subscripts g and l denote the gas phase and the liquid phase, respectively. This type of model with explicit account of interaction between fluids, see also (Tung and Dhir, 1988; Iliuta and Larachi, 2005), gives good results when compared with experimental results (Wang et al., 2013).

1.4. Outline of the study

Up to this point we have seen that the macroscopic momentum equations need the modeling of the force of interaction terms between phases. The interaction between fluids is neglected in the traditional model used for the study of subsurface two-phase flow, while it has been experimentally observed that these terms are important when studying two-phase flow in high permeability porous media. However, it is not known

whether these terms are always important when the extent of the interface between the fluids is important. For example, do they become negligible when friction with the solid phase increases? To what extent? To answer this question, we performed direct numerical simulations of two-phase flow in a Hele-Shaw cell as a model high permeability porous medium. We solved a coupled Level-Set and Stokes equations with an additional Darcy-term in the momentum equation that pertain for the absolute permeability of the flow between two plates. Thus, the friction due to the solid walls is increased by decreasing the aperture between the cell plates. This paper discusses the value of the interaction terms as a function of the aperture between the plates, i.e. the absolute permeability of the medium, and the capillary number and it is organized as follows. The following section 2 aims to introduce theoretical background about averaged quantities and two-phase displacement in a Hele-Shaw cell. In section 3 we present the numerical methods used to solve the flow and the free interface position. Finally, section 4 is devoted to the results, starting with the influence of the aperture between the plates on the distribution of fluids and pressure fields, and ending with the study of the traction terms.

2. Theorical background

2.1. Macroscopic quantities

In the following, the superficial average of a physical quantity θ_i associated with the i-phase is given by

$$\langle \theta_i \rangle = \frac{1}{V} \int_{V_i} \theta_i \, \mathrm{d}V. \tag{5}$$

Thus saturation and intrinsic average pressure for two fluids $i = w, o$ read

$$S_i = \frac{1}{V} \int_V \chi_i \, \mathrm{d}V$$

and

$$\langle p_i \rangle^i = \frac{\int_V p \chi_i \, \mathrm{d}V}{\int_V \chi_i \, \mathrm{d}V} = P_i,$$

respectively. In these equations V is the volume accessible to the fluids, that is the pore volume, and χ_i is the phase indicator of the i-fluid (scalar function that takes the value 1 in the fluid and 0 elsewhere). The quantity $\int_V \chi_i \ \mathrm{d}V$ is the volume fraction of the i-fluid that is ε_i and the intrinsic average ant the superficial average are linked as $\langle \theta_i \rangle = \varepsilon_i \langle \theta_i \rangle^i$.

Then we can introduce the dynamic capillary pressure defined as the difference of the intrinsic average pressures,

$$P_c = P_o - P_w. \tag{6}$$

2.2. Traction terms

An essential step in order to derive some macroscopic law at macroscale from the microscale is to use averaged quantities to express the exchange surface integrals terms. Remember that these closure relations are not presented here but rather we leave intact the surface integrals, the averaged momentum balance equations Eq. 2 for two fluids w

and o, are recast as

$$0 = -\varepsilon_w \nabla P_w + \mathbf{T}_{wo} + \mathbf{T}_{ws}, \tag{7a}$$

$$0 = -\varepsilon_o \nabla P_o + \mathbf{T}_{ow} + \mathbf{T}_{os}, \tag{7b}$$

where $\mathbf{T}_{ij}$ are the traction (name given to surface forces in the Boundary Integral Methods literature in which these integrals are central) exerted by fluid i upon fluid j and $\mathbf{T}_{is}$ the traction exerted by fluid i upon the solid (Kalaydjian, 1987). The traction terms are written as

$$\mathbf{T}_{ij} = \frac{1}{V} \int_{A_{ij}} \mathbf{n}_{ij} \cdot (-p_i \mathbf{I} + 2\mu_i \mathbf{e}_i) \, \mathrm{d}A, \tag{8}$$

where $\mathbf{n}_{ij}$ is the normal vector at the interface and pointing toward the j-phase, p_i the pointwise pressure of the fluid i and$\mathbf{e}_i = \frac{1}{2}\left(\nabla \mathbf{u}_i + (\nabla \mathbf{u}_i)^T\right)$ the rate-of-strain tensor for Newtonian fluids with $\mathbf{u}_i$ the pointwise velocity of fluid i.

2.3. Theory of two-phase displacement in Hele-Shaw cell

Displacement in a Hele-Shaw cell is a popular experimental set-up used to reproduced 2D potential flow similar to flow in porous media Guyon et al. (1994). Two-phase flow into such devices, as under study here, can be depicted as in Fig. 2. This represents a cocurrent flow of two fluids inside a Hele-Shaw cell parallel to the $x - y$ plane, with the z-axis perpendicular to the plates, and for which h is the aperture between the plates considered small in front of the other dimensions of the cell . A solid obstacle of cir-

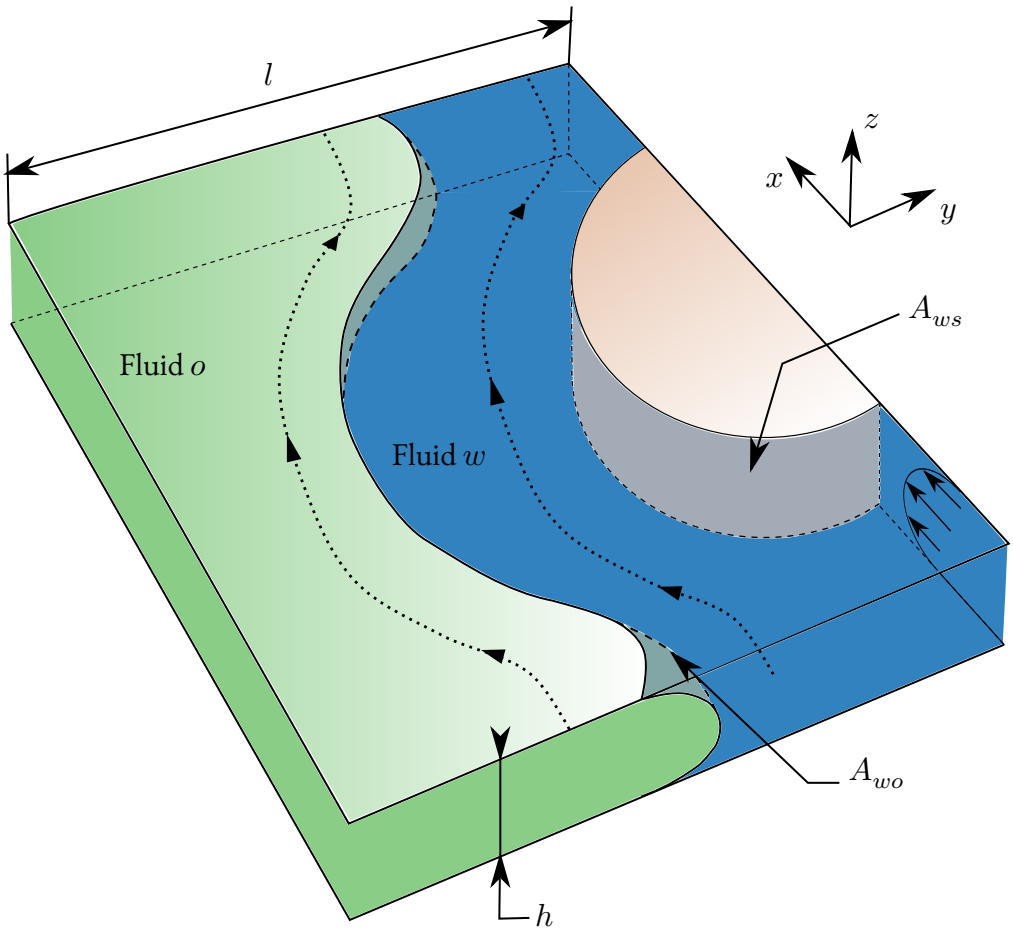

Figure 2: Illustation of confined cocurrent two-phase flow between two parallel plates and around cylinder obstacles.

cular cross-section is sandwiched between the two plates. Tangential (cell plane) stress, as well as stress arising from the perpendicular confinement, need to be taking into account to properly describe the flow. The important parameter here are the aspect ratio h/l where l is some characteristic transverse length (hereafter l is the cell width as shown in Fig. 2) and the capillary number.

To compute the traction exerted by the fluids upon the cell plates we consider that

the flow velocity is only oriented with the x-axis and that it depends only on the z-coordinate, where its profile follows the Poiseuille's law,

$$u = -\frac{1}{2\mu}\frac{dp}{dx}z(z-h).$$

Then the friction force exerted on the bottom plate is given by

$$\mu\frac{\partial u}{\partial z}\mid_{z=0} = -\frac{h}{2}\frac{dp}{dx}.$$

Thus, the traction $T^x_{i,pl}$ is obtained by multiplying the friction force by two times the surface wetted by the fluid i.

Going beyond the approximation that the velocity depends only on the z-coordinates we note that the average velocity taken over the interval between the plates is written as follows

$$\mathbf{U}(x,y,0) = -\frac{h^2}{12\mu}\nabla_{\parallel}p.$$

There is therefore a direct analogy between the flow in a 2D porous medium and the flow in a Hele-Shaw cell for which the permeability is given by $h^2/12$ (Saffman and Taylor, 1958). This allows us in the following to modify the absolute permeability of the structure without modifying its overall geometry, just by varying the aperture between the plates.

Beside the interface curvature in the Hele-Shaw cell plane, the meniscus in the perpendicular plane must be taken into account. Considering it as a semicircle of radius

$h/2$, the pressure jump at equilibrium across the interface reads

$$\Delta p = \gamma \left(\frac{2}{h} + \kappa_{\parallel} \right), \tag{9}$$

where γ denotes the surface tension and $\kappa_{\parallel}$ the curvature in the Hele-Shaw plane. Eq. 9 was completed by Park and Homsy (1984) with an additional term that pertains for dynamic film formation and a corrective $\pi/4$ factor for the curvature in the cell plane. The reader is warnes that while dynamic film formation along the plates is an important phenomenom regarding the flow (Jackson et al., 2015), this question requires dedicated study and is beyond the scope of this article. Thus, we consider in the following that the invading fluid is in contact with the cell plates, i.e. presence of a triple line.-

3. Direct numerical simulations

3.1. Equations

Level Set model

We used the standard Level Set method to capture the moving free interface between the fluids. The method is part of Eulerian methods which have the particularity of easily reproducing topological changes of the phases contrary to Lagrangian methods. As topological changes of the fluids is not excluded here, this motivated the choice for this type of method. In this framework the fluid phases are identified with a level set (scalar) function that goes smoothly from 0 to 1 across the fluid interface, which is implicitely defined as the iso-level $\phi = 0.5$. Transport of the level set function ϕ is

governed by

$$\frac{\partial \phi}{\partial t} + \nabla \cdot (\mathbf{u}\phi) = \tau \nabla \cdot \left(\psi \nabla \phi - \phi(1-\phi)\frac{\nabla \phi}{|\nabla \phi|} \right). \tag{10}$$

In this equation, $\mathbf{u}$ is the velocity field and τ and ψ are two numerical parameters that control the diffuse interface thickness and the amount of reinitialization of ϕ function, respectively (Olsson et al., 2007).

Flow equations

Remember that we need to take into account tangential stress as well perpendicular stress due to flow confinement, a full-3D resolution of flow equations would be meaningful. In order to avoid solving such resource-intensive simulations we rather resolved 2D flow equations plus an additional term taking into account the perpendicular stress. Velocity and pressure fields are obtained by solving 2D-modified Stokes equations since the Reynolds number is assumed to be sufficiently low so that the flow is creeping. The whole-domain formulation Stokes and continuity equations read

$$0 = -\nabla p + \mu(\phi)\left(\nabla^2 \mathbf{u} - k^2 \mathbf{u}\right) + \mathbf{F}_{st}, \tag{11a}$$

$$0 = \nabla \cdot \mathbf{u}, \tag{11b}$$

where $k = \frac{\sqrt{12}}{h}$ is an additional term that pertain to a Darcy-term arising from depth-averaging of Stokes equation, as described in the theoretical background section and $\mathbf{F}_{st}$ is the surface tension fore per unit volume. This term is defined here as a purely

normal contribution, i.e. constant surface tension along the interface, and reads

$$\mathbf{F}_{st} = \gamma\kappa\delta(\phi)\mathbf{n},$$

where $\mathbf{n}$ denotes the unit normal to the interface and $\delta(\phi)$ is the Dirac delta function localized on the interface (Sussman et al., 1994). In this framework the unit normal vector as well as the mean curvature are obtained with the level set function ϕ as

$$\mathbf{n} = \frac{\nabla\phi}{|\nabla\phi|}, \tag{12}$$

$$\kappa = \frac{\pi}{4}\nabla\cdot\left(\frac{\nabla\phi}{|\nabla\phi|}\right) + \frac{2}{h}, \tag{13}$$

respectively, where we added the $\pi/4$ factor in the curvature expression to be consistent with the correction derived by Park and Homsy (1984).

The fluid density and the fluid viscosity vary smoothly from one fluid to another

$$\rho(\phi) = \rho_o + (\rho_w - \rho_o)\phi,$$

$$\mu(\phi) = \mu_o + (\mu_w - \mu_o)\phi.$$

Dimensionless equations and relevant dimensionless numbers

If one define the following dimensionless variables

$$\mathbf{u} = \mathbf{u}' \times U,\ p = p' \times \frac{\mu U}{l},\ \kappa = \kappa' \times l,\ \mathbf{x} = \mathbf{x}' \times l,$$

where U is a reference velocity, μ a reference viscosity and l a reference length, Stokes and continuity equations can be recast as

$$0 = -\nabla' p' + \frac{\mu(\phi)}{\mu}\nabla'^2\mathbf{u}' + \frac{\gamma}{\mu U}\kappa'\nabla'\phi,$$

$$0 = \nabla' \cdot \mathbf{u}'.$$

One can notice the two following dimensionless numbers

$$\bar{\mu} = \frac{\mu(\phi)}{\mu},\ Ca^{-1} = \frac{\gamma}{\mu U},$$

the viscosity ratio and the capillary number, respectively, which add up to the aspect ratio h/l.

In the following, the results are given as a function of

$$Ca = \frac{(U_o + U_w)\mu_o}{\gamma}, \qquad U_w^{'} = \frac{U_w}{U_o + U_w} = f_f, \qquad U_o^{'} = 1 - f_f,$$

where f_f is called fractional flow, the reference viscosity is the invading fluid viscosity ($\mu_o = 2 \times \mu_w = 2 \times 10^{-3}$ Pa.s) and the reference velocity is the total velocity $U = U_o + U_w$. The viscosity ratio $\bar{\mu}$ as well as the fractional flow f_f are kept constant at 2 and 0.25, respectively, and the reference length is the cell's width denoted $l = 5 \times 10^{-4}$ m .

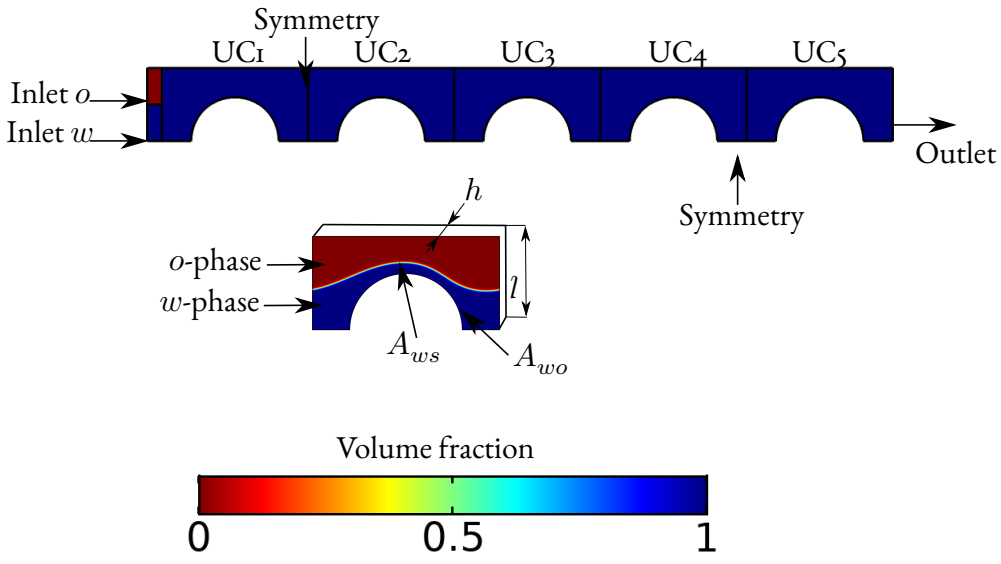

Figure 3: The geometry used is an array of 5 cylinders in a thin square cuboid, resembling a Hele-Shaw-cell where both fluids are injecting from left to right, initially the square cuboïd are saturated with wetting fluid (in blue), the length of one cell (UC) is one millimetre.

3.2. Geometry and boundary conditions

We study a model system consisting of an array of cylinders in a thin square cuboid, resembling a Hele-Shaw-cell with obstacles, as shown in Fig. 3. The two fluids are injected from the left at a constant normal velocity. The outlet boundary condition for the flow is a constant pressure. Initially the wetting fluid occupy the entire geometry. The different boundary conditions are listed in 1.

Boundary	$\mathbf{u}$	p	ϕ
A_{ws}	0	-	$\mathbf{n} \cdot \mathbf{u}\phi = 0$
Outlet	-	0	$\mathbf{n} \cdot \nabla\phi = 0$
Inlet o	$U_o^x = \text{cst}$	-	0
Inlet w	$U_w^x = \text{cst}$	-	1

Table 1: Boundary conditions

4. Results

Before we turn to the study of traction terms, we computed the absolute permeability of our model, remember that it is expected to be smaller than the $12/h^2$ value since the sandwiched cylinders contribute to the pressure drop along with the cell's plates. The absolute permeability of the model is varied by modifying the aperture between the two plates. We used five different values for the aperture and the correspondence in terms of absolute permeability, obtained from single-phase simulations, is given in Tab. 2. When $l/h \to \infty$, it is expected that the absolute permeability tends towards the permeability obtained for purely 2D flow, this is observed here since the absolute permeability for pure 2D case is 1.54×10^{-4} darcy which is very close to what we obtained for the largest aperture $h = 2.5 \times 10^{-3}$ m. Thus, the range of absolute permeability values is typical of what is encountered for high permeability porous media.

For the selected parameters, $f_f = 0.25$ and $0.05 < h^* < 5$, we observed only a film-flow regime without any phase rupture. The wetting fluid saturation in one cuboid, the third one in the rest of the paper unless otherwise specified, as a function of the dimensionless aperture and for different capillary numbers is given in Fig. 4 along

Table 2: Equivalence between the value of the cell plates aperture and the absolute permeability of the model obtained either from the $12/h^2$ value for flow between two plates or from single-phase simulation.

$h^* = h/l$	$h^2/12$ (darcy)	K (darcy)
5	5.2×10^5	1.5×10^4
0.5	5.2×10^3	2.8×10^3
0.25	1.3×10^3	8.6×10^2
0.125	3.3×10^2	2.3×10^2
0.05	5.2×10^1	3.9×10^1

with corresponding selected ϕ-fields. Wetting fluid saturation varies between 0.3 and 0.6 and increases as the aperture increases. The capillary number also impacts saturation by promoting the hold-up of the wetting fluid. As seen in the selected ϕ-fields, the smaller the capillary the flatter the interface. For a wetting fluid layer thickness equivalent at the plumb end of the cylinder, the saturation is logically higher.

Let us now take a closer look at the dynamic capillary pressure as expressed in Eq. and the pressure fields. Here, as can be seen in Fig. 5, the difference in intrinsic mean pressure of the fluids is entirely controlled by the pressure jump caused by the out-of-plane meniscus, even for the larger aperture, and does not depends on the capillary number at all. How the pressure jump compared to the pressure gradient across a cell? Based on the pressure fields in Fig. 6 one can answer that for $Ca = 1$ the pressure gradient across the cell is larger than the pressure jump and, interestingly, it becomes larger and larger than the pressure jump as the aperture between the plates is reduced. It is quite different when the capillary number decreases, and for $Ca = 0.01$ combined with a large aperture the pressure gradient across the cell is negligible in front of the pressure jump

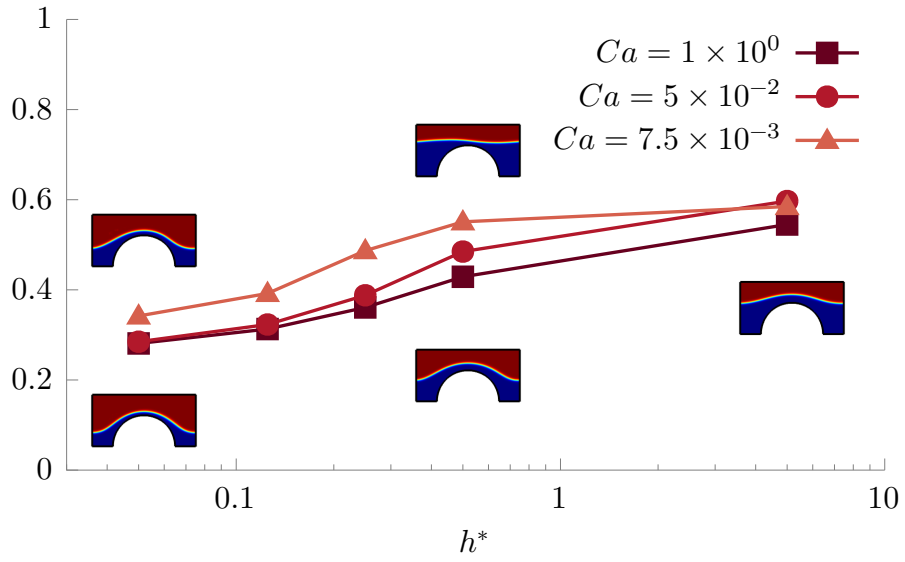

Figure 4: Wetting fluid saturation in UC_3 as a function of the dimensionless aperture between the Hele-Shaw plates and for different capillary numbers at steasy-state

due to surface tension effects. As the aperture decreases, the pressure gradient increases and becomes comparable to the pressure jump, but the pressure itsel is differently distributed in the cell compared to higher capillary number cases with a higher pressure in the wetting fluid.

We now turn to the study of the traction exerted upon the solid-fluid boundaries $\mathbf{T}_s$, i.e. fluid i upon the plates and wetting fluid upon the cylinder, along with the traction at the fluid-fluid interace $\mathbf{T}_f$. We focus on the magnitude of the traction exerted at the fluid-fluid interface compared to the traction exerted upon the solid boundaries. In the following we discuss only the x-component of the traction vector T^x, i.e. aligned according to the inlet velocity.

The traction exerted upont the plates by the fluids was obtained as described in

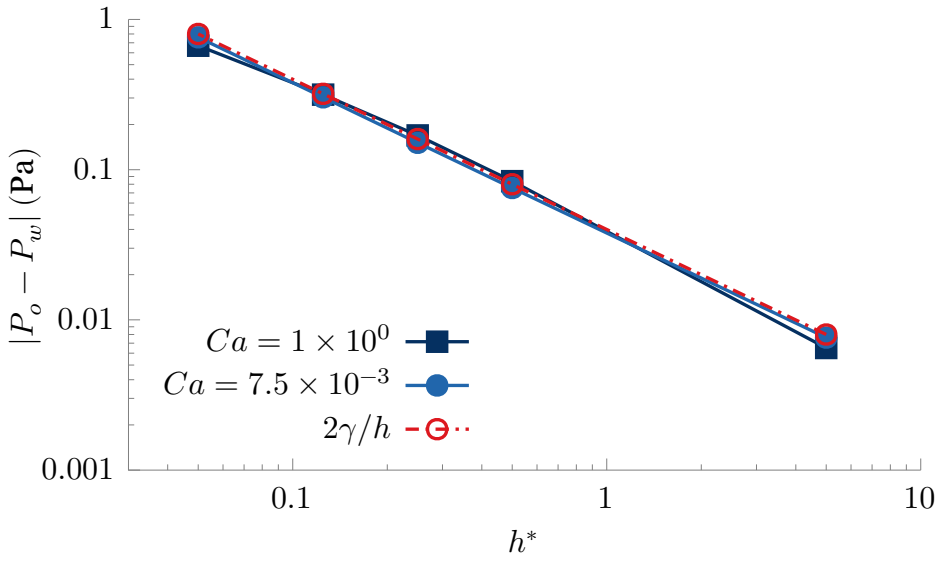

Figure 5: Dynamic capillary pressure in UC3 as a function of the dimensionless aperture between the Hele-Shaw cell plates, for different capillary numbers and pressure drop across the fluid-fluid from the out-of-plane meniscus at steady-state.

the theoretical backgound section. Traction on the cylinder boundary was obtained by calculating the integral Eq. 8. We computed the fluid-fluid traction $\mathbf{T}_f$ in two steps. The first step concerns the viscous part of the stress tensor, which was calculated directly from the velocity gradients available on the interface contour. The second step concerns the pressure part, which was obtained by applying the divergence theorem on each phase into a cell (UC3).

We assessed that the traction exerted on the fluid-fluid boundary reaches between 10 and 50% of the traction exerted upon the solid-fluid boundaries, as can be seen in Fig. 7, on which we plot the ratio T_f^x/T_s^x as a function of the dimensionless aperture between the cell plates. Interestingly, the ratio varies non-monotonically with h and the maximum value is obtained for the smallest aperture which then decreases when

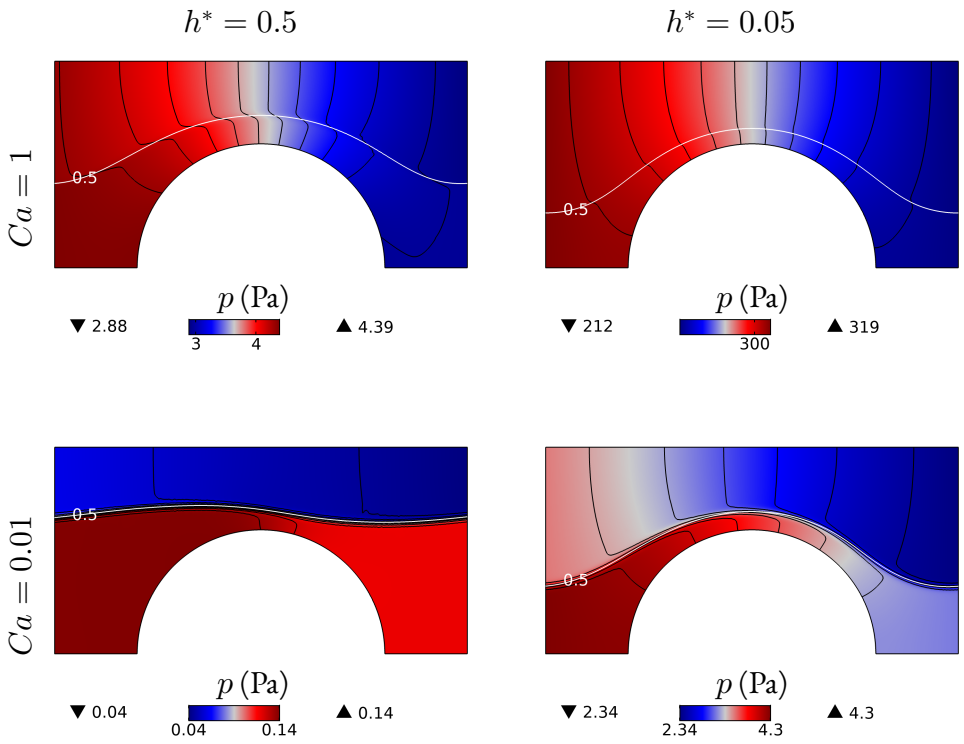

Figure 6: Pressure field in UC3 for two different capillary number and two different dimensionless apertures, interface position as the iso-ϕ=0.5 contour (white line) and isobar (black lines)

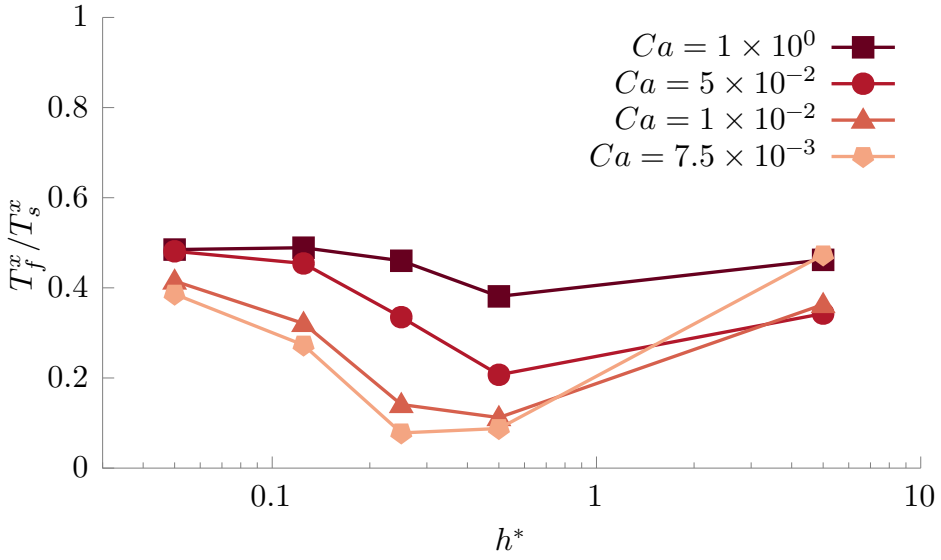

Figure 7: Ratio of traction (x-component) on fluid-fluid interface over traction on solid-fluid interfaces in UC_3 as a function of the dimensionless aperture between the Hele-Shaw plates and for different capillary numbers at steady-state.

the aperture increases. The capillary number accentuates the decrease of T_f^x compared to T_s^x when it decreases, as can be seen in Fig. 8.

Consider now the total traction on the fluid-fluid interface and the total traction exerted upon the solid boundaries plotted separately against the dimensionless aperture in Fig. 9. Between $h^* = 0.5$ and $h^* = 0.05$ the traction exerted upon the solid scale as h^{-2}, in contrast the traction at the fluid-fluid interface increases faster with h over the same interval. This explains why T_f^x/T_s^x increases as the aperture between the plates decreases. To go further we studied separately the pressure part and the viscous contribution in Eq.8 at the fluid-fluid interface as a function of the dimensionless aperture, see Fig. 10. For $h^* < 0.5$ the pressure part largely dominates the viscous contribution and the evolution of the traction is therefore controlled by it. The pressure part scales

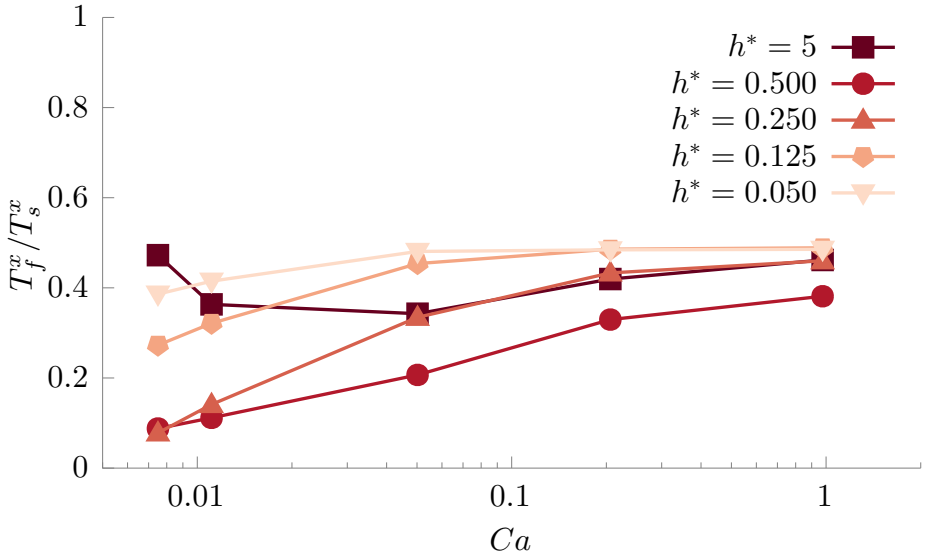

Figure 8: Ratio of traction (x-component) on fluid-fluid interface over traction on solid-fluid interfaces in UC_3 as a function of the capillary number and for different apertures at steady-state.

as h^{-2} for $Ca = 1$ but increases faster when the capillary number decreases.

Due to the proximity of the plates, the frictional forces are high, and they become higher and higher as they get closer. However, the traction exerted at the fluid/fluid interface does not become negligible compared to that exerted by the fluid upon the solid. Clearly, what is happening here is that the pressure increases due to the combination of constant inlet velocity and lower absolute permeability have a stronger effect on the traction term exerted at the fluid-fluid boundary. -

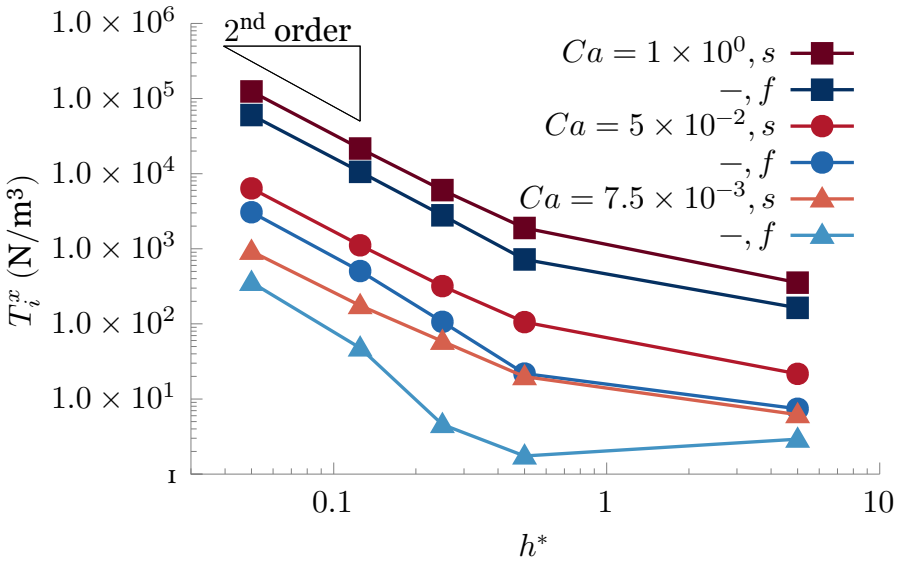

Figure 9: x-component of the traction exerted upon fluid-fluid interface and upon the solid-fluid interface in UC3 as a function of the dimensionless aperture between the Hele-Shaw plates and for different capillary numbers at steady-state.

Armstrong, R.T., McClure, J.E., Berrill, M.A., Rücker, M., Schlüter, S., Berg, S., 2016. Beyond darcy's law: The role of phase topology and ganglion dynamics for two-fluid flow. Physical Review E 94, 043113.

Attou, A., Boyer, C., Ferschneider, G., 1999. Modelling of the hydrodynamics of the cocurrent gas–liquid trickle flow through a trickle-bed reactor. Chemical Engineering Science 54, 785 – 802. doi:https://doi.org/10.1016/S0009-2509(98)00285-1.

Avraam, D.G., Payatakes, A.C., 1995a. Flow regimes and relative permeabilities during steady-state two-phase flow in porous media. Journal of Fluid Mechanics 293, 207–236. doi:10.1017/S0022112095001698.

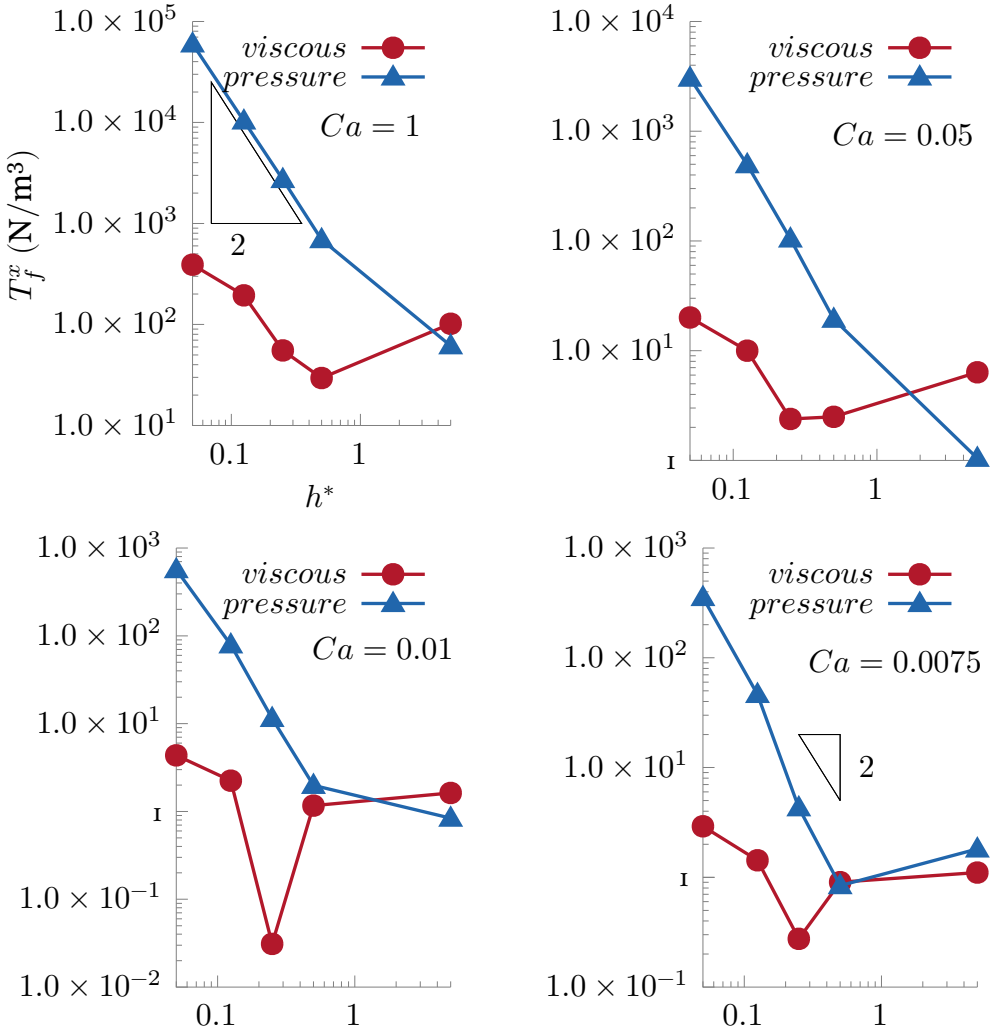

Figure 10: Viscous and pressure part of x-component of the traction exerted upon the fluid-fluid interface in UC_3 as a function of the dimensionless aperture between the Hele-Shaw plates at steady-state for different capillary numbers.

Avraam, D.G., Payatakes, A.C., 1995b. Generalized relative permeability coefficients during steady-state two-phase flow in porous media, and correlation with the flow mechanisms. Transport in Porous Media 20, 135–168. doi:10.1007/bf00616928.

Barenblatt, G.I., Patzek, T.W., Silin, D.B., 2003. The mathematical model of nonequilibrium effects in water-oil displacement. SPE journal 8, 409–416.

Bentsen, R.G., Manai, A.A., 1993. On the use of conventional cocurrent and countercurrent effective permeabilities to estimate the four generalized permeability coefficients which arise in coupled, two-phase flow. Transport in Porous Media 11, 243–262.

Blunt, M.J., 2017. Multiphase flow in permeable media: A pore-scale perspective. Cambridge University Press.

Clavier, R., Chikhi, N., Fichot, F., Quintard, M., 2017. Modeling of inertial multi-phase flows through high permeability porous media: Friction closure laws. International Journal of Multiphase Flow 91, 243–261.

Davit, Y., Quintard, M., 2018. One-phase and two-phase flow in highly permeable porous media. Heat Transfer Engineering , 1–19.

Dullien, F.A.L., 2012. Porous media: fluid transport and pore structure. Academic press.

Dullien, F.A.L., Dong, M., 1996. Experimental determination of the flow transport coefficients in the coupled equations of two-phase flow in porous media. Transport in Porous Media 25, 97–120. doi:10.1007/bf00141264.

Fetter, C.W., Boving, T., Kreamer, D., 2017. Contaminant hydrogeology. Waveland Press.

Guyon, E., Hulin, J.P., Petit, L., 1994. Hydrodynamique physique. interéditions.

Hassanizadeh, S.M., Gray, W.G., 1993. Thermodynamic basis of capillary pressure in porous media. Water Resources Research 29, 3389–3405. doi:10.1029/93WR01495.

Hilfer, R., 1998. Macroscopic equations of motion for two-phase flow in porous media. Physical Review E 58, 2090.

Iliuta, I., Larachi, F., 2005. Modelling the hydrodynamics of gas-liquid packed beds via slit models: A review. International Journal of Chemical Reactor Engineering 3.

Jackson, S., Stevens, D., Giddings, D., Power, H., 2015. Dynamic-wetting effects in finite-mobility-ratio hele-shaw flow. Physical Review E 92, 023021.

Kalaydjian, F., 1987. A macroscopic description of multiphase flow in porous media involving spacetime evolution of fluid/fluid interface. Transport in Porous Media 2, 537–552. doi:10.1007/BF00192154.

Langaas, K., Papatzacos, P., 2001. Numerical investigations of the steady state relative permeability of a simplified porous medium. Transport in Porous Media 45, 241–266.

Lasseux, D., Quintard, M., Whitaker, S., 1996. Determination of permeability tensors

for two-phase flow in homogeneous porous media: theory. Transport in Porous Media 24, 107–137.

Leverett, M., et al., 1941. Capillary behavior in porous solids. Transactions of the AIME 142, 152–169.

Li, H., Pan, C., Miller, C.T., 2005. Pore-scale investigation of viscous coupling effects for two-phase flow in porous media. Physical Review E 72. doi:10.1103/physreve.72.026705.

Muskat, M., 1938. The flow of homogeneous fluids through porous media. Soil Science 46, 169.

Odeh, A.S., et al., 1959. Effect of viscosity ratio on relative permeability (includes associated paper 1496-g) .

Olsson, E., Kreiss, G., Zahedi, S., 2007. A conservative level set method for two phase flow ii. Journal of Computational Physics 225, 785 – 807. doi:https://doi.org/10.1016/j.jcp.2006.12.027.

Park, C.W., Homsy, G., 1984. Two-phase displacement in hele shaw cells: theory. Journal of Fluid Mechanics 139, 291–308.

Ramakrishnan, T.S., Goode, P.A., 2015. Measurement of off-diagonal transport coefficients in two-phase flow in porous media. Journal of colloid and interface science 449, 392–398.

Rose, W., 1988. Measuring transport coefficients necessary for the description of coupled two-phase flow of immiscible fluids in porous media. Transport in Porous Media 3, 163–171. URL: https://doi.org/10.1007/BF00820343, doi:10.1007/BF00820343.

Rothman, D.H., 1990. Macroscopic laws for immiscible two-phase flow in porous media: Results from numerical experiments. Journal of Geophysical Research 95, 8663. doi:10.1029/jb095ib06p08663.

Saffman, P.G., Taylor, G.I., 1958. The penetration of a fluid into a porous medium or hele-shaw cell containing a more viscous liquid. Proceedings of the Royal Society of London. Series A. Mathematical and Physical Sciences 245, 312–329.

de Santos, J.M., Melli, T.R., Scriven, L.E., 1991. Mechanics of gas-liquid flow in packed-bed contactors. Annual Review of Fluid Mechanics 23, 233–260. doi:10.1146/annurev.fl.23.010191.001313.

Shams, M., Raeini, A.Q., Blunt, M.J., Bijeljic, B., 2018. A study to investigate viscous coupling effects on the hydraulic conductance of fluid layers in two-phase flow at the pore level. Journal of colloid and interface science 522, 299–310.

Sussman, M., Smereka, P., Osher, S., 1994. A level set approach for computing solutions to incompressible two-phase flow. Journal of Computational Physics 114, 146 – 159. URL: http://www.sciencedirect.com/science/article/pii/S0021999184711557, doi:https://doi.org/10.1006/jcph.1994.1155.

Tung, V., Dhir, V., 1988. A hydrodynamic model for two-phase flow through porous media. International Journal of Multiphase Flow 14, 47 – 65. URL: http://www.sciencedirect.com/science/article/pii/030193228890033X, doi:https://doi.org/10.1016/0301-9322(88)90033-X.

Wang, Y., Chen, J., Larachi, F., 2013. Modelling and simulation of trickle-bed reactors using computational fluid dynamics: A state-of-the-art review. The Canadian Journal of Chemical Engineering 91, 136–180. URL: https://onlinelibrary.wiley.com/doi/abs/10.1002/cjce.20702, doi:10.1002/cjce.20702, arXiv:https://onlinelibrary.wiley.com/doi/pdf/10.1002/cjce.20702.

Whitaker, S., 1986. Flow in porous media II: The governing equations for immiscible, two-phase flow. Transport in porous media 1, 105–125.

Wyckoff, R.D., Botset, H.G., 1936. The flow of gas-liquid mixtures through unconsolidated sands. Physics 7, 325–345.

Yiotis, A.G., Psihogios, J., Kainourgiakis, M.E., Papaioannou, A., Stubos, A.K., 2007. A lattice boltzmann study of viscous coupling effects in immiscible two-phase flow in porous media. Colloids and Surfaces A: Physicochemical and Engineering Aspects 300, 35 – 49. doi:https://doi.org/10.1016/j.colsurfa.2006.12.045. proceedings of the Fourth International TRI/Princeton Workshop.

Zarcone, C., Lenormand, R., 1994. Détermination expérimentale du couplage visqueux dans les écoulements diphasiques en milieu poreux. Comptes rendus de l'Académie des sciences. Série II, Mécanique, physique, chimie, astronomie 318, 1429–1435.

AppendixA. Model validation

The code is validated by comparison with a Boundary-Element Method, which relies on a surface discretization of the interface and a pseudo-analytical formulation in the bulk of the phases. This allows us to precisely locate the interface, even in the case of very thin film flow, and to carefully analyze the choice of parameters in Eq. 10.